Spreading dynamics of drop impacts

Guillaume Lagubeau[1], **Marco A. Fontelos**[2], **Christophe Josserand**[3]†,
Agnès Maurel[4], **Vincent Pagneux**[1] **and Philippe Petitjeans**[5]

[1] LAUM, UMR CNRS 6613, Avenue Olivier Messiaen, 72085 Le Mans CEDEX 9, France

[2] Instituto de Ciencias Matemáticas, (ICMAT, CSIC-UAM-UC3M-UCM), C/ Serrano 123,
28006 Madrid, Spain

[3] Institut D'Alembert, CNRS & UPMC (Université Paris 06), UMR 7190, case 162, 4 place Jussieu,
75005 Paris, France

[4] Institut Langevin, LOA, UMR CNRS 7587, ESPCI, 10 rue Vauquelin, 75005 Paris, France

[5] PMMH, UMR CNRS 7636, ESPCI, 10 rue Vauquelin, 75005 Paris, France

We present an experimental study of drop impact on a solid surface in the spreading regime with no splashing. Using the space–time-resolved Fourier transform profilometry technique, we can follow the evolution of the drop shape during the impact. We show that a self-similar dynamical regime drives the drop spreading until the growth of a viscous boundary layer from the substrate selects a residual minimal film thickness. Finally, we discuss the interplay between capillary and viscous effects in the spreading dynamics, which suggests a pertinent impact parameter.

Key words: drops, drops and bubbles, interfacial flows (free surface)

1. Introduction

Drop impact is characteristic of multiphase flows (Rein 1993). It is present for instance in atomization processes (Eggers & Villermaux 2008), raindrop dynamics (Planchon & Mouche 2010), inkjet printing (Zable 1977) and micro-fabrication (Antkowiak *et al.* 2011), but it also involves most of the key issues of surface flows (Peregrine 1981). Depending on the dynamical properties and whether the impacted surface is a thin liquid film, a thick liquid film or a solid substrate, drop impact can lead to prompt splashing, corona splashes or rapid spreading. In particular, for impact on a liquid film or bath, prompt splashes are observed for high impact speeds (Worthington 1908; Yarin & Weiss 1995), while the splash is suppressed for lower speeds, leading to vortex ring and cavity formation for a deep pool (Rein 1996) and crater-like deformation for a thin liquid film (Deegan, Brunet & Eggers 2008; Lagubeau *et al.* 2010). When the drop impacts on a dry solid substrate, different outcomes are also possible (Rioboo, Marengo & Tropea 2001): again, at high speed, splashing is observed, and it has recently been shown that such a splash could be suppressed by decreasing the surrounding gas pressure (Xu, Zhang & Nagel 2005), indicating a genuine influence of the gas. On the other hand, at lower velocity, the droplet shape exhibits strong deformation at the substrate contact (Renardy *et al.* 2003); then the drop spreads on the solid up to a maximum radius and eventually

† Email address for correspondence: josseran@lmm.jussieu.fr

retracts due to capillary forces. Depending on the wetting properties, the retraction can lead to an equilibrium spherical cap, a rebound of the drop (Bartolo, Josserand & Bonn 2005) or even singular jets (Bartolo, Josserand & Bonn 2006).

In this paper, we consider a drop of diameter $D = 2R_0$ that impacts at velocity V_0 on a flat solid surface. Drop behaviour is determined by two dynamical dimensionless numbers, the Reynolds number (Re), which balances inertia with viscous effects, and the Weber number (We), which balances inertia with capillary effects:

$$Re = \frac{DV_0}{\nu} \quad \text{and} \quad We = \frac{\rho DV_0^2}{\gamma}, \tag{1.1}$$

where ν, ρ and γ are the kinematic viscosity, the liquid density and the surface tension coefficient respectively. The solid properties are only of marginal influence on the spreading behaviour in the case of sufficiently high Weber number considered here (Clanet *et al.* 2004). The different regimes of impact dynamics are summarized in figure 1. Of particular interest is the spreading regime, where no splashing or jetting is present and where the surrounding gas can be neglected in the dynamics. This regime has recently been investigated, and it has been shown that the drop spreads by forming a flat central area surrounded by a growing rim until the surface tension and/or the viscous forces finally stop this expansion (Clanet *et al.* 2004; Roisman 2009; Eggers *et al.* 2010; Schroll *et al.* 2010). The droplet relaxes to an equilibrium shape or to a partial/total rebound of the drop, depending on the wetting properties. For high velocity, splashing is observed (Rioboo *et al.* 2001), while spreading is observed for smaller velocities where capillary waves can make the drop bounce (Biance *et al.* 2006), sometimes even leading to singular jets (Bartolo *et al.* 2006). A so-called splashing parameter K has been proposed to characterize the transition between the spreading (low K) and the splashing (high K) regime (Mundo, Sommerfeld & Tropea 1995):

$$K = We\sqrt{Re}. \tag{1.2}$$

In the spreading case, particular attention has been paid to the scaling of the maximum radial expansion where different regimes have been identified, depending on the balance between inertia, capillarity and viscous forces (Roisman, Rioboo & Tropea 2002; Clanet *et al.* 2004; Bartolo *et al.* 2005; Fedorchenko, Wang & Wang 2005). An impact number P separating capillary-limited expansion (low P) from viscous-limited expansion (large P) has been defined. It can be written in the form $P = We\,Re^\alpha$, and we expect $\alpha < 0$, in contrast to the splashing parameter K, since high P values correspond to viscous-limited expansion. Nevertheless, since only intermediate values of impact number can be reached experimentally, in the capillary regime it has not yet been possible to discriminate between a model based on a capillary-selected pancake expansion $P_w = We\,Re^{-4/5}$ (Clanet *et al.* 2004) and one based on the surface energy balance $P_e = We\,Re^{-2/5}$ (Eggers *et al.* 2010). Finally, neither existing experiments nor numerical simulations have been able to give a comprehensive scenario of the spreading dynamics. This is mainly due to a lack of precise interface measurements experimentally and the limitations of numerical simulations, for instance because of the difficulty of modelling the moving contact line.

2. Experimental setup

We studied the impact of a liquid drop on a flat hydrophobic surface, consisting of Parafilm M, chosen for its low contact angle hysteresis and good hydrophobicity
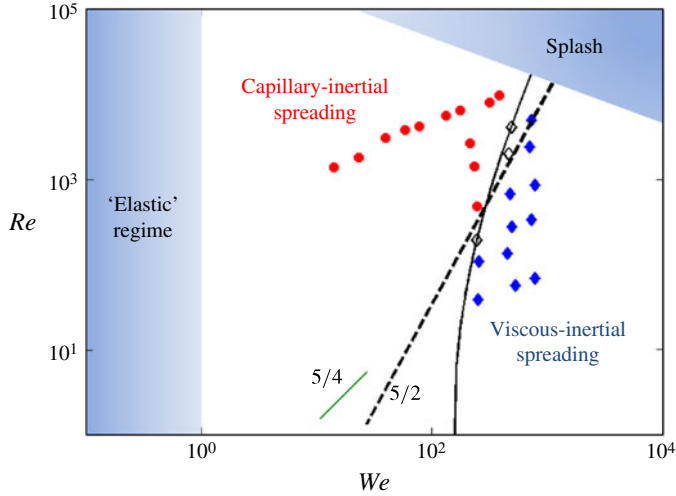
FIGURE 1. (Colour online) Different drop impact regimes. The splashing (Mundo *et al.* 1995) and 'elastic regime' (low *We*) (Biance *et al.* 2006) zones are delimited qualitatively. Our displayed experiments are within these limits. The spreading can be dominated by viscous (blue diamonds, $\tau_r > 1.05\tau_p$) or capillary (red circles, $\tau_r < 0.95\tau_p$) inertia balance. The boundary between these behaviours is indicated by the empty diamonds ($1.05\tau_p > \tau_r > 0.95\tau_p$) and the black line (the empirical law (4.3)).

(measured equilibrium contact angle $98 \pm 5°$), stretched over a 5 cm × 5 cm optical flat mirror. The results obtained here are valid for general surface properties The drop of controlled diameter, ranging from 3.3 to 4.1 mm, detached from a syringe and then fell freely from a height ranging between 3 and 60 cm. With the use of seven different water–glycerol mixtures, viscosity was varied by two orders of magnitude (0.95, 3.0, 6.0 18.0, 44.0, 80.7 and 220.4 mPa s respectively). Water was freshly deionised (Milli-Q) and glycerol was provided by Aldrich (Rectapur 99 %). A temperature-controlled room was used for achieving good stability of the liquid properties for the whole duration of the experiments.

The space–time-resolved Fourier transform profilometry technique (FTP) was used to measure the drop shape (Takeda & Mutoh 1983; Maurel *et al.* 2009). A high-resolution video projector (Epson TW5500) projects over the measurement surface a one-dimensional fringe pattern whose deformations are recorded by a fast camera (Phantom v9.0) and compared to the pattern projected over a flat reference. We used the parallel optical configuration described in Takeda & Mutoh (1983) and Maurel *et al.* (2009): the two optical axes are coplanar and parallel to each other, separated by $D = 21$ cm, while the entrance pupils are positioned at the same height L (75 cm) over the undeformed reference surface as shown in figure 2. This technique was recently fitted to the study of fast liquid surface deformations (Cobelli *et al.* 2009, 2011*a,b*; Chekroun *et al.* 2012). The fringe wavelength over the measurement surface was 1.1 mm, four times smaller than the drop diameter before impact, thus avoiding the intrinsic band-limitation of the FTP technique. The height resolution for each measurement point over a grid of 100 μm mesh size was 20 μm. Angular averaging around the impact point (determined by fitting an ellipse to the drop contour just before the impact) improved the resolution of the mean height profile to a typical value of 5 μm. A very low concentration (0.2 % in volume) of white
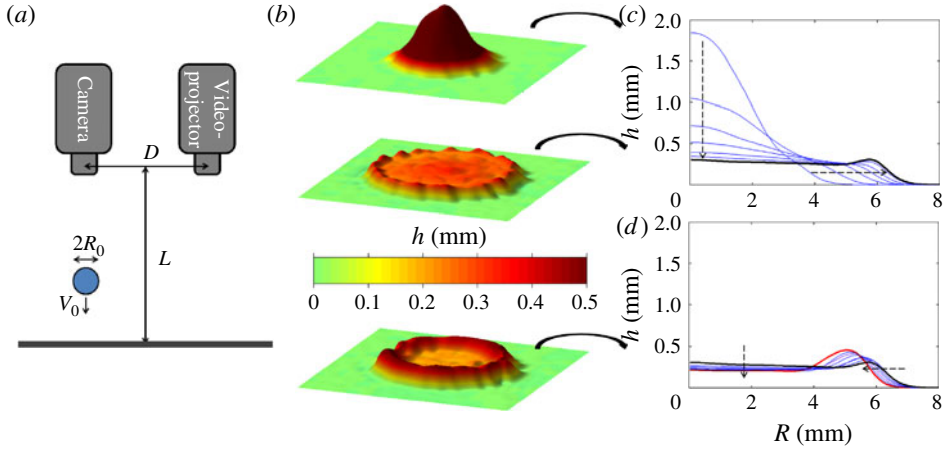
FIGURE 2. (Colour online) Evolution of drop shape with time for a 50.17 %$_{wt}$ water–glycerol drop of radius 1.98 mm impacting a Parafilm surface at a speed of 1.91 m s^{-1} ($We = 235$ and $Re = 1413$). (*a*) Experimental setup. (*b*) Height mapping of the drop for an early time ($t = 3, 5$ ms, top), the maximal radial expansion ($t = 10.3$ ms, middle) and the minimal thickness ($t = 19.7$ ms, bottom). (*c,d*) Successive drop profiles of the same experiment. The time step is 0.74 ms. (*c*) Successive profiles up to the maximal lateral expansion symbolized by the bold black line. (*d*) Successive profiles from top to bottom between the maximal lateral expansion and the minimal thickness (bold black line and bold red line, respectively, online).

pigment (Kronos1001) was added to the liquid to enhance the light diffusion by the interface, while the surface tension and the viscosity remained unchanged (Przadka *et al.* 2012). The pigment concentration was tuned so that fringe contrast over the liquid and the Parafilm surface were equivalent.

Experiments with a drop eccentricity before impact lower than 0.95 due to detachment oscillations were eliminated. The time interval between two successive images was set to 740.5 μs, and we interpolated the impact time ($t = 0$) with a resolution of 0.1 ms using the drop velocity and height on the image, before the impact was measured directly using FTP. Four independent experiments for each different viscosity and falling height were used to give a single curve improving the time resolution by a factor of four.

3. Temporal sequence of the drop shape dynamics and minimal thickness of the inner film

The spreading dynamics is illustrated in figure 2, where the evolution of the interface profiles is shown for $D = 3.96$ mm and $V_0 = 1.91$ m s^{-1}. Figure 2(*b*) shows three snapshots of the interface heights measured with FTP techniques. Wiggles are visible in these three-dimensional patterns because of FTP band-limitation and measurement uncertainties. Nevertheless, the axisymmetry of the surface shape is correctly preserved, and measurement artifacts are suppressed by performing an angular average of the height, $\bar{h}(r, t) = 1/(2\pi) \int_0^{2\pi} h(r, \theta, t)\, d\theta$, where r and θ are the usual cylindrical coordinates, presented in figure 2(*c,d*). Figure 2(*c*) represents the spreading dynamics (where the spreading radius of the liquid patch increases in time) and figure 2(*d*) shows the retracting dynamics (the spreading radius decreases). Meanwhile, the central part of the liquid patch flattens in time and eventually
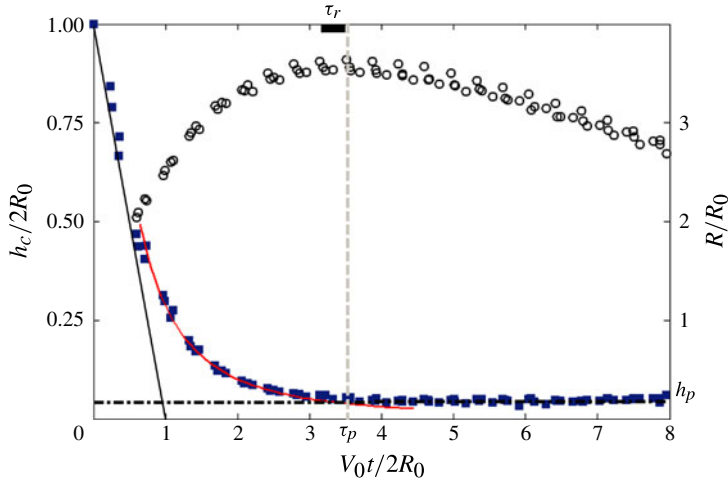
FIGURE 3. (Colour online) Squares and left vertical axis: height h_c of the top of the central point of the drop surface as a function of time for $We = 214$ and $Re = 2690$. Circles and right vertical axis: radius of expansion R of the same drop. The solid line indicates the freefall regime. The red curve is the best fit of $h_c(t) = AD^3/(V_0^2 (t + t_0)^2)$ during the self-similar regime and the black dash-dotted line corresponds to the plateau h_p; τ_p (vertical dashed line) is the crossing time between the two latter regimes, and τ_r is the time of the maximal lateral expansion with an error bar indicated by the black segment.

converges towards a constant film thickness h_p (called the minimal film thickness later on). Three distinct dynamical regimes of spreading can be identified in the detailed time evolution of the film thickness at $r = 0$ ($h_c(t)$, shown in figure 3): the early time regime is a linear decrease corresponding to the freefall of the top of the drop. For large times, h_c clearly tends to the constant h_p. The transition between these two regimes corresponds to an intermediate phase where the interface velocity decreases. Eventually, the drop retracts because of surface tension, a fourth dynamical regime that is not considered here. For low Weber numbers ($We < 40$ while $Re > 1000$) no plateau is observed, since h_c rebounds immediately after reaching its minimum value. These three regimes have in fact already been described theoretically and numerically (Roisman 2009; Eggers *et al.* 2010), and have the following features.

Pressure impact. A strong pressure field is induced close to the impact region, evidence of the deviation of the vertical velocity of the drop into a horizontal field, similar to the pressure impulse observed in liquid impacts (Cooker & Peregrine 1995). In this regime, the drop apex continues falling at the impact velocity V_0 until the pressure impact reaches the top of the drop (approximately $V_0 t = R_0$), in good agreement with the linear decrease observed in figure 3.

Self-similar inertial regime. The evolution of the drop can be modelled using a thin film approximation, considering a potential flow matched with a boundary layer on the solid surface. This theory shows that the drop shape $h(r, t)$ exhibits a self-similar behaviour followed by a viscous regime where the minimal thickness is limited by the growth of the boundary layer. In order to keep the paper self-contained, we recall here the principal steps of these analytical works. After the impact and before the viscous-dominated regime, the flow inside the drop is described by a hyperbolic (potential) solution corresponding to a stagnation point induced by the impact, $v_r = r/t$ and $v_z = -2z/t$, where v_r and v_z are the radial and vertical velocities. The time t can
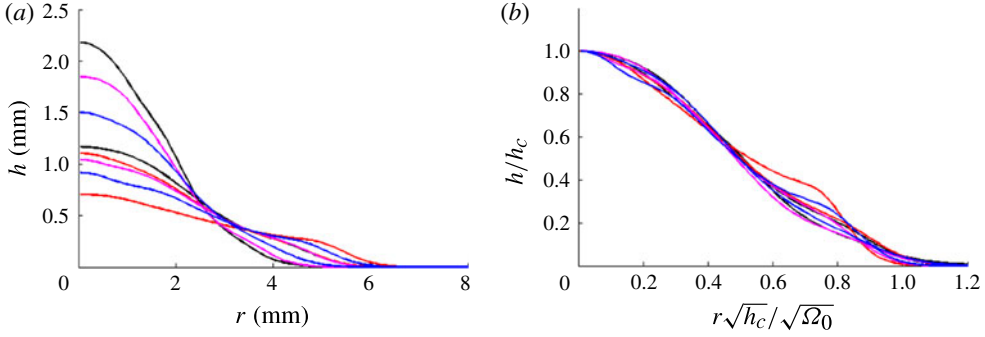
FIGURE 4. (Colour online) (*a*) Series of drop profiles at times 1.14, 1.25, 1.34, 1.5, 1.52, 1.62, 1.71 and 1.87 in the non-dimensionalized time unit for $We = 255$ and $Re = 1470$, each colour corresponding to one experiment. (*b*) Collapse of the same profiles using the self-similar variables h/h_c and $r\sqrt{h_c}/\sqrt{\Omega_0}$, with h_c the height of the centre of the drop and Ω_0 its volume.

be replaced in this solution by $t + t_0$, where t_0 accounts for the delay between the onset of the impact with the self-similar regime (it is expected to be of the order of D/V_0). The drop deforms while spreading on the surface, according to $\partial_t h + v_r \partial_r h = v_z$, and this latter equation admits a self-similar generic solution:

$$h(r, t) = \frac{D^3}{V_0^2 (t + t_0)^2} H\left(\frac{r}{V_0(t + t_0)}\right). \tag{3.1}$$

This self-similar behaviour is not expected to be valid at small times (a pressure impact regime where h_c decreases linearly) or large times (a viscous-dominant regime with constant film thickness h_p), but it is a good candidate for describing the intermediate regime. Such a law can be tested experimentally, after advantageously reformulating (3.1) as $h(r, t) = h_c G(r\sqrt{h_c}/\sqrt{\Omega_0})$, in order to get rid of the unknown parameter t_0 (Ω_0 being the drop volume). Figure 4 exhibits good collapse of the drop shapes at different times (figure 4*a*) into a single curve (figure 4*b*) by plotting $h(r, t)/h_c$ as a function of $r\sqrt{h_c}/\sqrt{\Omega_0}$. As expected, we notice that the quality of the collapse fails for large times, initially around the contact line. Moreover, (3.1) predicts the central height of the drop to be

$$h_c(t) = A\frac{D^3}{V_0^2 (t + t_0)^2}, \tag{3.2}$$

where $A = H(0)$ is a constant. This law is compared with the experimental results collated for different Re and We in figure 5, where the interface central height h_c is shown as function of time on logarithmic scales. There, we observe the collapse of all the curves for short times, and fitting this master curve with the theoretical law (3.2), we find $A = 0.492 \pm 0.030$ and $V_0 t_0/D = 0.429 \pm 0.033$ (red curves in figures 3 and 5). For larger times, the experiments deviate from the curve because of viscous effects, exhibiting the plateau regime where the height h_c converges toward the constant value h_p. This process depends only on the Reynolds number, as shown in the inset of figure 5.

Plateau regime. The end of film thinning was understood within the thin film model as a viscous correction to the hyperbolic flow. When viscosity is accounted
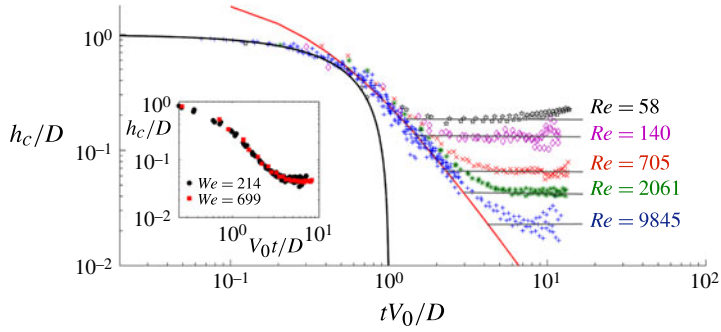
FIGURE 5. (Colour online) Logarithmic plot of the evolution of h_c with time for different Reynolds numbers and similar Weber numbers $(Re, We) = (9845, 382)$, $(2061, 467)$, $(705, 479)$, $(140, 449)$ and $(58, 539)$ respectively. Black solid line, ballistic regime; red dotted line, self-similar regime; black dotted lines, plateau regime (h_p). The inset shows the evolution of h_c in time for similar Reynolds numbers but different Weber numbers $(2690, 214)$ and $(2440, 699)$.

for, a viscous boundary layer is found to grow from the substrate with a thickness l_v classically following $l_v \sim \sqrt{\nu t}$. Therefore, interpreting the asymptotic film thickness h_p as the merging of this boundary layer with the drop surface, we obtain for the asymptotic film thickness h_p and the cross-over time t_p (defined as the intersection time of the two asymptotic behaviours):

$$h_p \sim Re^{-2/5}D \quad \text{and} \quad t_p \sim Re^{1/5}D/V_0. \tag{3.3}$$

Notice that this scaling for h_p is obtained by taking the particular (hyperbolic) internal flow inside the drop introduced above. Although this flow is physically pertinent, it should be compared to a simpler scaling considering the growth of a boundary layer only over the typical impact time D/V_0 which would give $h_p \sim Re^{-1/2}R_0$, which exhibits an exponent in the Reynolds number very close to the other exponent (0.5 versus 0.4)! This minimal film thickness is important in the context of coating or inkjet printing but no experimental evidence has been provided so far, in particular because the film thickness could not be measured to a high degree of accuracy. On the numerical side, full simulations of the Navier–Stokes equations with a free surface condition have not been able to discriminate clearly between the two scalings, in particular because of numerical limitations related to the contact line dynamics (Eggers *et al.* 2010; Schroll *et al.* 2010). However, a simplified model of the impact dynamics deduced from the numerical simulations suggests that the $-2/5$ law (3.3) is valid (Eggers *et al.* 2010).

In our shape measurements, the slope of the inner region is below 1 % in the plateau regime so that h_c gives an accurate measurement of h_p. Figure 6 shows the variation of h_p with the Reynolds number, h_p being computed as the mean value of h_c in the plateau regime. The best fit of the measures gives $h_c \propto Re^{-0.422\pm0.028}$, in good quantitative agreement with the 2/5 law. Similarly, figure 7 shows the dimensionless cross-over time $\tau_p = V_0 t_p/D$ as a function of $Re^{1/5}$, in good agreement with the law (3.3). In fact, a linear fit gives
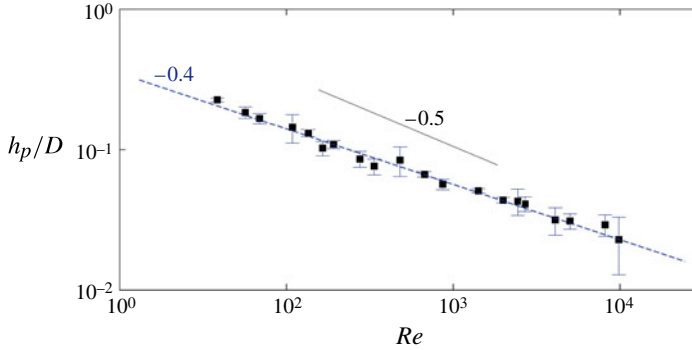
$$\tau_p = aRe^{1/5} + \tau_{c0}, \tag{3.4}$$

FIGURE 6. (Colour online) Minimal thickness of the inner film h_p as a function of the Reynolds number Re. The two suspected laws $Re^{1/2}$ and $Re^{2/5}$ are shown as a guide.
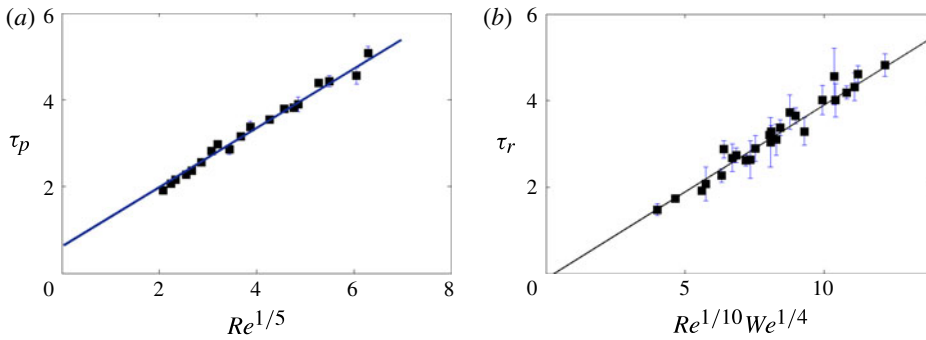

FIGURE 7. (Colour online) (*a*) Dimensionless cross-over time $\tau_p = V_0 t_p/D$ between inertial and viscous regimes in the central layer as a function of $Re^{1/5}$. (*b*) Dimensionless time of the maximal radial expansion τ_r as a function of $Re^{1/10}We^{1/4}$.

with $a = 0.71 \pm 0.04$ and $\tau_{c0} = 0.53 \pm 0.16$, reminiscent of the delay due to the pressure impact phase. Finally, let us emphasize that the scaling for τ_p in $Re^{1/5}$ is the same as the law obtained for the maximum spreading expansion in the viscous regime (Clanet *et al.* 2004).

4. Capillary and/or viscous balance

It is interesting to compare this cross-over time t_p, which indicates when viscous effects decrease the spread of drop impact with the time of maximum expansion t_r, which is dependent on a balance between inertia, viscous forces and capillarity. Indeed, when $t_p \gg t_c$, one can expect the maximum radius to be dominated by the capillary–inertia balance, while it should be dominated by a viscous–inertia balance in the opposite limit. As stated in §1, an impact parameter P based on the maximum expansion radius has already been proposed. It distinguishes a capillary–inertia balance (low P) from a viscous–inertia one (high P), but its detailed expression is still a matter of debate between two possible expressions P_w and P_e. On one hand, considering that capillary waves select the expanding drop thickness, we obtain $P_w = We/Re^{4/5}$ (Clanet *et al.* 2004). On the other hand, the balance between the initial kinetic energy

and the surface energy at maximum expansion gives the other impact parameter $P_e = We/Re^{2/5}$ (Eggers *et al.* 2010). Ironically, the range of parameters available experimentally does not allow us to discriminate between these two approaches, while a numerically based model suggests that the energy balance parameter P_e is the pertinent one. It is thus tempting to characterize the spreading as the ratio between these two times: t_r/t_p.

Although the FTP band-limitation smooths the side of the profile, an accurate measurement of the spreading radius can be obtained as the position of the maximal profile slope. Then, R_{max} and t_r are determined by fitting a parabola on a limited time interval close to the maximum expansion time, giving 1 and 10 % error bars for R_{max} and t_r respectively. The dimensionless time $\tau_r = V_0 t_r/D$ is observed to depend on both *We* and *Re*. An empirical scaling $\tau_r \propto Re^{1/10}$ is found for each of the three sets of fixed Weber numbers experiments, and finally, all the data collapse well when drawn as a function of $Re^{1/10}We^{1/4}$, as shown in figure 7. Following this scaling, the best fit gives

$$\tau_r = bRe^{1/10}We^{1/4} + \tau_{r0}, \tag{4.1}$$

with $b = 0.42 \pm 0.04$ and $\tau_{r0} = -0.25 \pm 0.32$. From the fitting laws (3.4) and (4.1) we can deduce an empirical law for the impact parameter in the asymptotic limit ($Re \gg 1$ and $We \gg 1$),

$$\frac{t_r}{t_p} \sim 0.59 \frac{We^{1/4}}{Re^{1/10}} \sim 0.59 P_e^{1/4}, \tag{4.2}$$

suggesting that P_e is the relevant impact parameter, as shown already by a numerical approach in Eggers *et al.* (2010).

For intermediate values of *We* and *Re*, the initial times τ_{r0} and τ_{c0} are relevant,

$$\frac{t_r}{t_p} = \frac{bRe^{1/10}We^{1/4} + \tau_{r0}}{aRe^{1/5} + \tau_{c0}}, \tag{4.3}$$

where τ_{c0} (close to 0.5) can be understood as the flow-establishing time after the impact, while τ_{r0} is the spreading time at zero velocity, which one would expect to be zero, consistent with our estimate. In figure 1, the different experiments are summarized in the (Re, We) plane, with red circles when $t_r/t_p < 1.05$ and blue diamonds when $t_r/t_p > 0.95$. A dashed line $P_e = $ const. is drawn that describes the data better than the green segment $P_w = $ const. In fact we observe good agreement between the two criteria ($P_e = $ const. and $t_r/t_p = 1$) in the range of the experiment although only intermediate values of impact parameters can be reached ($4 < Re^{1/10}We^{1/4} < 12$, and $2.5 < Re^{1/5} < 6.3$). The weak power-law dependence of τ_r and τ_p in *We* and *Re* makes the asymptotic regime difficult to reach experimentally, regardless of the fact that for such high impact splashing would occur.

5. Conclusion

In conclusion, we would like to emphasize that, using the FTP technique, several key quantitative measurements concerning the shape evolution sequence of the spreading drop have been obtained, namely: (i) the self-similar expansion of the drop shape predicted in (Eggers *et al.* 2010); (ii) the minimal film thickness scaling like $Re^{-2/5}$; (iii) the transition time between these two regimes scaling like $Re^{1/5}$; (iv) lastly, the ratio between the time of maximal expansion τ_r and the time of the plateau regime τ_p suggesting that P_e is the crucial impact parameter, and that the drop expansion in the inviscid limit is controlled by the balance between kinetic and surface energies.

Acknowledgements

REFERENCES

ANTKOWIAK, A., AUDOLY, B., JOSSERAND, C., NEUKIRCH, S. & RIVETTI, M. 2011 Instant fabrication and selection of folded structures using drop impact. *Proc. Natl Acad. Sci. USA* **108**, 10400–10404.

BARTOLO, D., JOSSERAND, C. & BONN, D. 2005 Retraction dynamics of aqueous drops upon impact on nonwetting surfaces. *J. Fluid Mech.* **545**, 329–338.

BARTOLO, D., JOSSERAND, C. & BONN, D. 2006 Singular jets and bubbles in drop impact. *Phys. Rev. Lett.* **96**, 124501.

BIANCE, A., CHEVY, F., CLANET, C., LAGUBEAU, G. & QUÉRÉ, D. 2006 On the elasticity of an inertial liquid shock. *J. Fluid Mech.* **554** (1), 47–66.

CHEKROUN, M., MAUREL, A., LAGUBEAU, G., PAGNEUX, V., COBELLI, P., PRZADKA, A. & PETITJEANS, P. 2012 Space–time resolved experiments for water waves. *Acta Polonica* **120** (61), 142–148.

CLANET, C., BÉGUIN, C., RICHARD, D. & QUÉRÉ, D. 2004 Maximal deformation of an impacting drop. *J. Fluid Mech.* **517**, 199–208.

COBELLI, P., MAUREL, A., PAGNEUX, V. & PETITJEANS, P. 2009 Global measurement of water waves by Fourier transform profilometry. *Exp. Fluids* **46** (6), 1037–1047.

COBELLI, P., PAGNEUX, V., MAUREL, A. & PETITJEANS, P. 2011*a* Experimental study on water-wave trapped modes. *J. Fluid Mech.* **666**, 445–476.

COBELLI, P., PRZADKA, A., PETITJEANS, P., LAGUBEAU, G., PAGNEUX, V. & MAUREL, A. 2011*b* Experimental investigation of different regimes for water wave turbulence. *Phys. Rev. Lett.* **107**, 214503.

COOKER, M. & PEREGRINE, D. 1995 Pressure-impulse theory for liquid impact problems. *J. Fluid Mech.* **297**, 193–214.

DEEGAN, R. D., BRUNET, P. & EGGERS, J. 2008 Complexities of splashing. *Nonlinearity* **21** (1), C1–C11.

EGGERS, J., FONTELOS, M., JOSSERAND, C. & ZALESKI, S. 2010 Drop dynamics after impact on a solid wall: theory and simulations. *Phys. Fluids* **22**, 062101.

EGGERS, J. & VILLERMAUX, E. 2008 Physics of liquid jets. *Rep. Prog. Phys.* **71**, 036601.

FEDORCHENKO, A., WANG, A.-B. & WANG, Y.-H. 2005 Effect of capillary and viscous forces on spreading of a liquid drop impinging on a solid surface. *Phys. Fluids* **17**, 093104.

LAGUBEAU, G., FONTELOS, M., JOSSERAND, C., MAUREL, A., PAGNEUX, V. & PETITJEANS, P. 2010 Flower patterns in drop impact on thin liquid films. *Phys. Rev. Lett.* **105**, 184503.

MAUREL, A., COBELLI, P., PAGNEUX, V. & PETITJEANS, P. 2009 Experimental and theoretical inspection of the phase-to-height relation in Fourier transform profilometry. *Appl. Opt.* **48**, 380–392.

MUNDO, C., SOMMERFELD, M. & TROPEA, C. 1995 Droplet–wall collisions: experimental studies of the deformation and breakup process. *Intl J. Multiphase Flow* **21**, 151–173.

PEREGRINE, D. 1981 The fascination of fluid mechanics. *J. Fluid Mech.* **106**, 59–80.

PLANCHON, O. & MOUCHE, E. 2010 A physical model for the action of raindrop erosion on soil microtopography. *Soil Sci. Soc. Am. J.* **74**, 1092–1103.

PRZADKA, A., CABANE, B., PAGNEUX, V., MAUREL, A. & PETITJEANS, P. 2012 Fourier transform profilometry for water waves: how to achieve clean water attenuation with diffusive reflection at the water surface? *Exp. Fluids* **52** (2), 519–527.

REIN, M. 1993 Phenomena of liquid drop impact on solid and liquid surfaces. *Fluid Dyn. Res.* **12**, 61–93.

REIN, M. 1996 The transitional regime between coalescing and splashing drops. *J. Fluid Mech.* **306**, 145–165.

RENARDY, Y., POPINET, S., DUCHEMIN, L., RENARDY, M., ZALESKI, S., JOSSERAND, C., DRUMRIGHT-CLARKE, M., RICHARD, D., CLANET, C. & QUÉRÉ, D. 2003 Pyramidal and toroidal water drops after impact on a solid surface. *J. Fluid Mech.* **484**, 69–83.

RIOBOO, R., MARENGO, M. & TROPEA, C. 2001 Outcomes from a drop impact on solid surfaces. *Atomiz. Sprays* **11**, 155–165.

ROISMAN, I. 2009 Inertia dominated drop collisions. Part 2. An analytical solution of the Navier–Stokes equations for a spreading viscous film. *Phys. Fluids* **21**, 052104.

ROISMAN, I., RIOBOO, R. & TROPEA, C. 2002 Normal impact of a liquid drop on a dry surface: model for spreading and receding. *Proc. R. Soc. Lond.* A **458** (2022), 1411–1430.

SCHROLL, R., JOSSERAND, C., ZALESKI, S. & ZHANG, W. 2010 Impact of a viscous liquid drop. *Phys. Rev. Lett.* **104**, 034504.

TAKEDA, M. & MUTOH, K. 1983 Fourier transform profilometry for the automatic measurement of 3-D object shapes. *Appl. Opt.* **22**, 3977–3982.

WORTHINGTON, A. 1908 *A Study of Splashes*. Macmillan (reprinted in 1963).

XU, L., ZHANG, W. & NAGEL, S. 2005 Drop splashing on a dry smooth surface. *Phys. Rev. Lett.* **94**, 184505.

YARIN, A. & WEISS, D. 1995 Impact of drops on solid surfaces: self-similar capillary waves, and splashing as a new type of kinematic discontinuity. *J. Fluid Mech.* **283**, 141–173.

ZABLE, J. L. 1977 Splatter during ink jet printing. *IBM J. Res. Dev.* **21** (4), 315–320.